Asia-Pacific Journal of Atmospheric Sciences
https://doi.org/10.1007/s13143-019-00136-7

Online ISSN 1976-7951
Print ISSN 1976-7633

ORIGINAL ARTICLE

A Comparative Study on the Effect of Upstream Trough on Intensity Changes of Two Types of Tropical Cyclones during Extratropical Transition

Yue Liao[1,2,3,4] · Yongqing Wang[1,2,3,4] · Jialing Zhou[4,5] · Xiunian Zhang[6]

Received: 25 October 2018 / Revised: 19 May 2019 / Accepted: 27 May 2019

Abstract

Based on the China Meteorological Administration (CMA) tropical cyclone (TC) database and the reanalysis data from the European Centre for Medium-Range Weather Forecasts (ECMWF), the post-transition intensifying tropical cyclones (ITC) and weakening tropical cyclones (WTC) which landed in China and underwent extratropical transition (ET) are discussed in this paper. The TCs with upper-level trough are selected in order to identify different effects of the trough on the ITC and the WTC. The dynamic composite analysis is applied to explore their structure characteristics, environment fields and dynamic diagnosis. Results show that affected by the South Asia high and the subtropical high, the trough of ITC (WTC) extends from northwest to southeast (northeast to southwest) in the ET process. Thus, the zonal wind shear of ITC drops off after ET due to the approach of trough and its northwest-southeast direction, while the zonal and total wind shears of WTC continue to increase because of the steering westerly flow at the upper level. In terms of the ITC, the cold air carried by the upper-level trough intrudes into TC inner area and mostly encircles the TC center, making the ITC characterized by a warm seclusion. While for the WTC, the cold air only wanders on the northwest side of TC without further intrusion. The upper-level divergence is also in favor of the ITC by the pumping influence. According to the diagnostic analysis of moist potential vorticity, the moist baroclinity can lead to changes in vertical vorticity to some extent. The vertical vorticity budget analysis further indicates that there is stronger and wider positive vorticity advection in the upper troposphere near the TC center for ITC. The contribution of the baroclinic term to the growth of vertical vorticity is more significant in ITC than WTC but it is also deeply influenced by the strength of upper-level trough.

Keywords Tropical cyclone · Extratropical transition · Composite analysis · Upstream trough · Baroclinity · Vorticity budget

Responsible Editor: Kyong-Hwan Seo.

Electronic supplementary material The online version of this article (https://doi.org/10.1007/s13143-019-00136-7) contains supplementary material, which is available to authorized users.

✉ Yongqing Wang
yongqing@nuist.edu.cn

[1] Collaborative Innovation Center on Forecast and Evaluation of Meteorological Disasters, Nanjing University of Information Science & Technology, Nanjing 210044, China

[2] Key Laboratory of Meteorological Disaster, Ministry of Education, Nanjing University of Information Science & Technology, Nanjing 210044, China

[3] School of Atmospheric Sciences, Nanjing University of Information Science & Technology, Nanjing 210044, China

[4] Nanjing Joint Center of Atmospheric Research, Nanjing 210009, China

[5] Jiangsu Research Institute of Meteorological Sciences, Nanjing 210009, China

[6] Yunnan Meteorological Observatory, Kunming 650034, China

Published online: 14 June 2019

1 Introduction

The extratropical transition (ET) of tropical cyclones (TC) can be described as the propagation of a TC into the mid-latitudes where it interacts with a preexisting mid-latitude cyclone or a midlevel trough and the following transition into an extratropical cyclone (Kofron et al. 2010a). It has been found that some extratropical cyclones even have greater strength than TCs, and may also cause threats similar to that of TCs such as gale, heavy rain and flood. Park et al. (2016) also displayed that damages by ETs are as much as those by TCs in northwestern provinces of the Republic of Korea. So far, they are proved difficult to forecast but have not received enough attention. Klein et al. (2000) revealed that TCs undergoing ET all exhibited a common series of structure changes, including the increasing temperature gradient with colder temperatures to the north, as well as the enhanced vertical wind shear and baroclinity. The ET process was described by a conceptual model and divided into two stages, i.e., transformation stage and extratropical stage. Moreover, several definitions of the ET time have been proposed based on TC characteristics during the ET process (Evans and Hart 2001; Hart 2003; Harr and Elsberry 2000; Demirci et al. 2007; Kofron et al. 2010b).

Previous studies have indicated that the upper-level trough might have a significant impact on both of the transformation stage and the extratropical stage. Li and Xu (2012) revealed a well corresponding relationship between the variation of TC intensity after ET and the initial strength of the westerly upper-level trough, and they investigated the impacts of different troughs on Haima's reintensification by using the method of piecewise potential vorticity (PV) inversion. Likewise, McTaggart-Cowan et al. (2001) simulated the ET process and reintensification of Hurricane Earl in 1998 in order to examine its sensitivity to modification of PV anomaly. It was suggested that the existence of an upstream trough is of primary importance to the storm's reintensification, while the presence of the low-level circulation associated with the decaying hurricane plays a secondary role. Atallah and Bosart (2003) suggested that the distribution and intensity of the TC precipitation are also strongly modulated by the storm's interaction with a mid-latitude trough. Baek et al. (2014) simulated the ET process of Typhoon Rusa in 2002 and further revealed that the antecedent mid-tropospheric frontogenesis, which is resulted from the interaction between the typhoon and a mid-latitude trough over the Korean Peninsula, could contribute to the first peak in the time series of rainfall in Gangneung. Ritchie and Elsberry (2003) conducted three control simulations without a TC present to examine the extratropical cyclogenesis associated with upper-level troughs that are characterized as weak, moderate, and strong. When no TC is included in the simulation, the minimum surface pressures with the weak, moderate, and strong troughs are 1003, 991, and 977 hPa, respectively. Subsequently, the impact of phasing between TCs and trough on reintensification of TCs were detected by fixing the initial position and amplitude of the mid-latitude trough and varying the initial position of the TC to trough (Ritchie and Elsberry 2007). It was indicated that the peak intensity of the extratropical cyclone following the ET is strongly dependent on the phasing which could lead to different extents of interaction between TCs and mid-latitude baroclinic zones.

The potential vorticity theory and its application have become booming since 1980s (Shou 2010). The "PV thinking" perspective has been proved effective in studies of transitioning TCs (e.g., McTaggart-Cowan et al. 2001; Atallah and Bosart 2003; Thorncroft and Jones 2000; Browning et al. 2000), with advantages as follows. (1) The maximum of PVs in the upper troposphere features cold-core systems (mid-latitude troughs), which is favorable to trace the upper-level cold air and reveal the interaction between TCs and upper-level troughs. (2) The PV is conserved without regard to the friction and diabatic. It is necessary to take the water vapor into consideration in the mechanism analysis of rainfall especially rainstorms, and therefore, the moist potential vorticity (MPV) was proposed (Shou 2010). Based on studies on rainstorm mesoscale cyclogenesis, Shou and Li (2001) indicated that the absolute vorticity could increase as the upper cold air with large MPV slides down along the moist isentropic surface, which tends to cause the cyclogenesis. In view of the MPV conservation principle, the low-level cyclonic circulation can be triggered by the downward-propagated upper MPV, which is beneficial for vortex development (Ying et al. 2013). In order to analyze the explosive cyclone development and its relationship with MPV, the MPV was calculated by the barotropic and baroclinic components, respectively. Results showed that the connection of negative values of baroclinic MPV in the high and low troposphere might be of benefit for the cyclone development, and the cyclone develops faster with the stronger atmospheric baroclinity (Niu et al. 2003). Wu and Cai (1995, 1997) proposed that with the slant of moist isentropic surface the reduction of convective stability, the increase of the vertical shear of horizontal wind or moist baroclinity can result in the increase of vertical vorticity, no matter the atmosphere is moist symmetrically stable or unstable, or convectively stable or unstable. The development of vertical vorticity intends to be more vigorous with the larger declination of moisture isentropes. Above studies suggested that the downward extension of the moist potential vorticity related to the upper-level trough can increase the positive vorticity at the lower level and hence induce the cyclonic circulation.

In this paper, the post-transition intensifying tropical cyclones (ITCs) and weakening tropical cyclones (WTCs) which landed in China and underwent ET with the presence of upstream upper-level trough are examined. We apply the dynamic composite analysis to detect the basic structure characteristics, synoptic environment and relative diagnostics. In section 2, the data and methods are described. Section 3–4

provide the result analysis. A summary and conclusion are presented in section 5.

2 Data and Methods

TCs' path and intensity information in this paper are obtained from the China Meteorological Administration (CMA) Tropical Cyclone Best Track Dataset. There are 755 extratropical cyclones transformed from tropical storm over the western North Pacific in the period of 1987 to 2016, with 32 of them landing in China. According to Li and Xu (2012), an index was defined as the difference that TC minimum surface pressure after ET time minus the TC center pressure 6 h before the ET time. If the index is less than 0 hPa, the TC is defined as ITC, If the index is greater than 0 hPa, it is classified as WTC. According to the statistics, there are 10 ITCs and 19 WTCs in the samples. Finally, 5 ITCs and 7 WTCs are selected in the current study, which are 9219, 9711, 0108, 0421, 1010 for ITC and 9216, 9415, 0102, 0515, 0601, 0713, 1410 for WTC. The criteria of selection are illustrated as follows. (1) In order to reduce errors caused by regional differences in the composite analysis, the location where the ET is first completed should be within the area of 119°E-131°E, 32°N-45°N. (2) Both types of TCs are accompanied with upper-level upstream troughs. (3) CMA marks the extratropical cyclone with the number "9″, and the majority of TCs were stopped decoding after the third "9″ appeared. Therefore, in order to ensure the uniformity, intensity changes of the TCs should occur within 12 h after the ET. The tracks of ITCs and WTCs are shown in Fig. 1, with the black dots representing the locations at the initial time of ET completion, i.e., "ET time". We express the "ET time" as "Te" in the following figures, and 6 h before and after "ET time" as "Te-6″ and "Te+6″, respectively.

The analyses of environment fields, structure characteristics and dynamic diagnoses in this paper are all based on the dynamic composite technique (Li 2004), taking the center of TC as the center of coordinate, which can keep the TC circulation and its surrounding pattern relatively intact. In addition, the standard deviation of composite analysis between samples is supplemented in Online Resource (Fig. S1-S8) in order to make the results more valid. The data for composite analysis are obtained from ECMWF reanalysis data with the horizontal resolution of 0.5° × 0.5°.

3 Basic Structure Characteristics of ITC and WTC

3.1 Planetary Scale

The planetary scale (approximately 40° latitude×50° longitude box around the TC center) circulation and thermodynamic characteristics were examined in this section. It can be seen from the composite background fields at 200 hPa that the upper-level trough exists to the northwest of both ITC and WTC at "Te-12". The upper jet stream is located in front of the trough with its wind speed larger than 30 m s^{-1}, and the distinct divergence zone exists on the right side of the jet entrance. Note that the composite geopotential height field illustrates that the South Asia high with the value of 12,520 gpm exists not only in the ITC but also in the WTC (Fig. 2a and d). It can be also inferred from Fig. 2a and d that the coverage and strength of the South Asia high for WTC are greater than those for the ITC. After 12 h, the South Asia high for ITC weakens and retreats westward under the influence of the upper-level trough moving eastward. In such case, the trough and the poleward TC are more close without any obstacles, and the ITC is adjacent to the upper divergence zone on the north side. In the process of the upper-level trough for WTC moving eastward, due to the intensity inferior to the South Asia high, the movement is impeded and slows down. Meanwhile, the WTC divergence decreases significantly and it is gradually away from TC center (shown in Fig. 2b and e). At 12 h after the completion of ET, the upper-level trough for

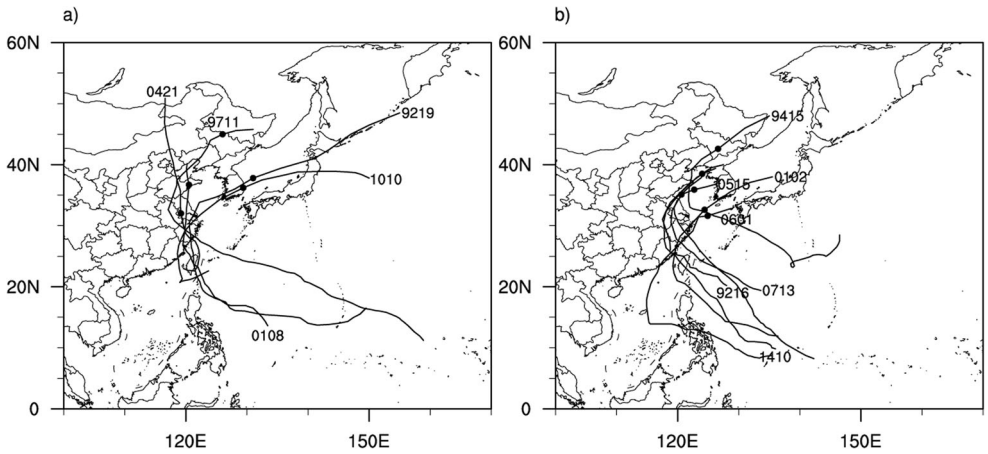

Fig. 1 Tracks of (**a**) ITCs and (**b**) WTCs (black dots indicate the locations at the initial time of ET completion, i.e., "ET time")

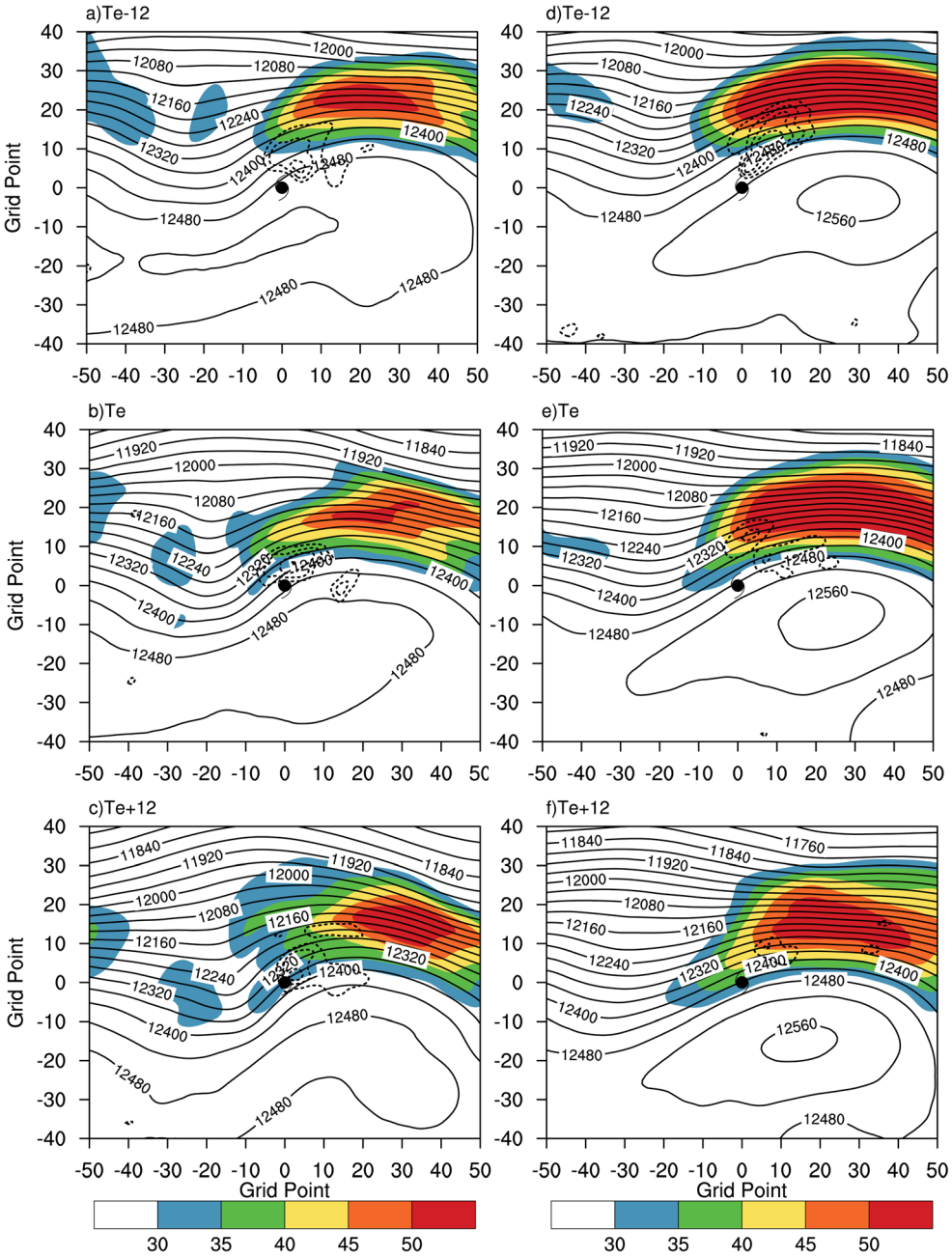

Fig. 2 Composite horizontal distribution of the upper-level jet (shaded, units: m s^{-1}), the geopotential height (black lines, units: gpm) and the divergence larger than 2×10^{-5} s^{-1} (black dashed contours, interval of 1×10^{-5} s^{-1}) of (**a**-**c**) ITC and (d-f) WTC at 200 hPa at the time of (**a**, **d**) Te-12, (**b**, **e**) Te and (**c**, **f**) Te+12. The coordinate origin is the TC center (northward and eastward are referred positive, westward and southward are referred negative) and the horizontal resolution is 0.5° × 0.5°

ITC extends southeastward further so that the South Asia high withdraws southward quickly. The trough stretches from northwest to southeast and the strong poleward airflow in front of the trough accelerates the TC's poleward moving into the divergence zone on the right side of the Westerly Jet entrance. The upper divergent over TC center provides a favorable pumping environment for ITC's reintensification. Nevertheless, blocked by the South Asia high, the upper-level trough for WTC remains stagnant, and thus the trough extends to the southwest more significantly. Under the circumstances, the WTC dominated by the westerly airflow moves northward at a slower speed and gradually away from the divergence zone (Fig. 2c and f). The illustration above is also evident for the composite geopotential height field at 500 hPa, where the extension and strength of jet for WTC far exceeds those for ITC (not shown), which can account for the trough's stagnation to some extent.

The composite equivalent potential temperature at 850 hPa and the composite temperature advection at 700 hPa are shown in Fig. 3. Although the ET locations of TCs differ from each other, the temperature fields are set with the TC center as the coordinate center. In other words, for a TC system, the surrounding temperature distribution does not differ significantly for the location (as shown in Fig. S9, S10 in Online Resource). At "Te-12", the temperature difference between the cold dry air

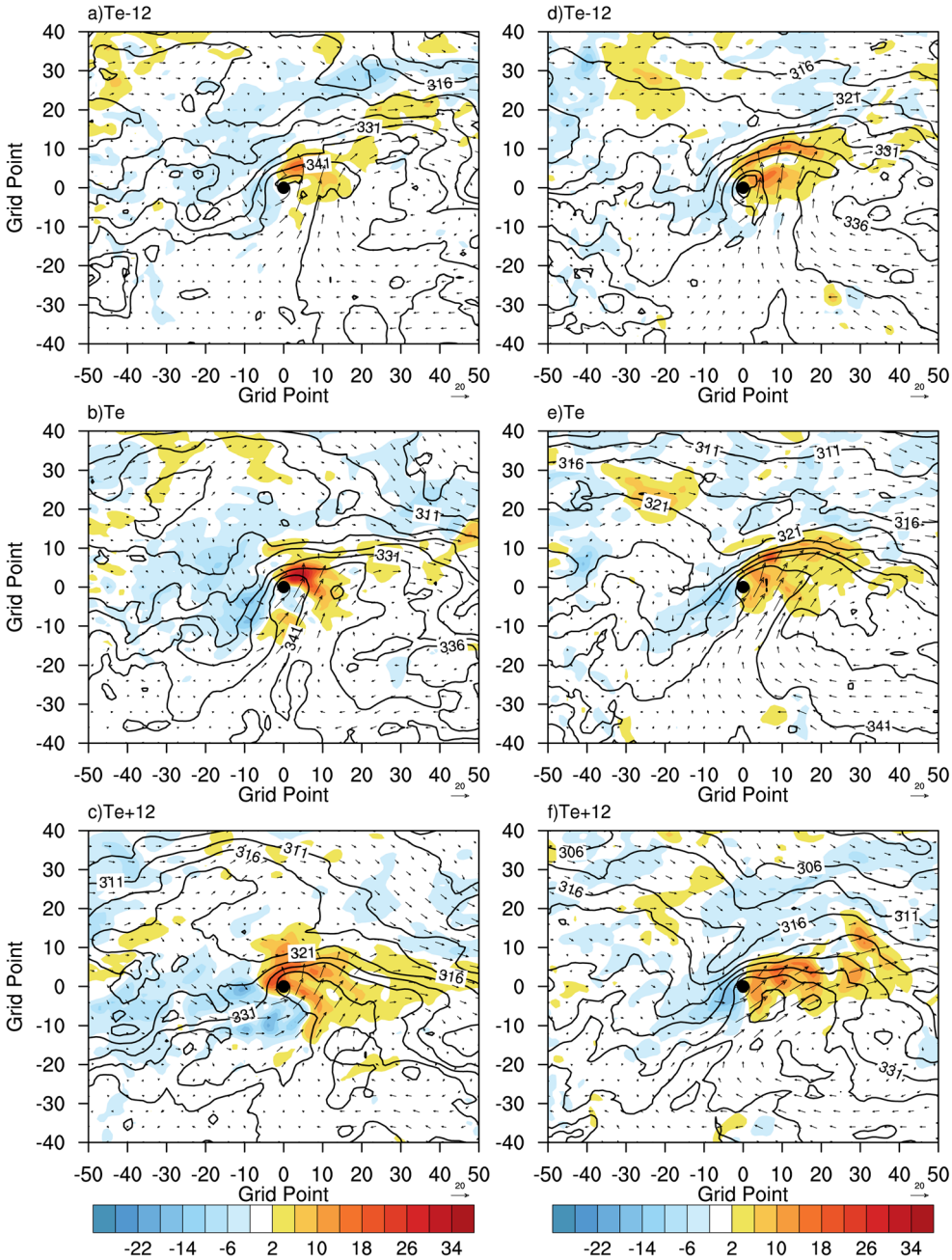

Fig. 3 Same as Fig. 2, but for the equivalent potential temperature (black contours, units: K) at 850 hPa, the temperature advection (shaded, units: 1×10^{-5} K s^{-1}) and the wind vector (wind barb, units: m s^{-1}) at 700 hPa

to the northwest side of TC and the warm moist air of residual TC makes the isentropes denser on the north side of TC for both ITC and WTC. The warm advection brought by the poleward airflow occurs on the eastern part of TC, and the northerly airflow on the west side moves southward with cold air. In this paper, the value of equivalent potential temperature less than 336 K was defined to trace the cold air, which is found located to the northern and western parts of the TC (Fig. 3a and d). At "Te", the cold air from the northern part of TCs moves further southward. The cold air for ITC intrudes into the TC from west to southwest, accompanied with greater cold advection. However, the cold air for WTC remains in the west of the TC without obvious southward movement (Fig. 3b and e). After 12 h, it is indicated from Fig. 3c and d that the cold advection is modulated by the ITC's cyclonic circulation from southwest to southeast, which also encircles the TC center in a semi-circular shape. The cold air for WTC still lingers on northwest and southwest sides of TC and does not move southward further. The process of the cyclonic cold airflow encircling the ITC center presented in the low-level equivalent potential temperature field is consistent with the "warm seclusion" characteristic mentioned in Section 3.2 (Fig. 5c), which is conductive to the re-emergence of warm core and thus plays a role in the reintensification of ITC.

3.2 Synoptic Scale

In this section, the structure characteristics are explored at the synoptic scale (approximately 10° × 10° around the TC center). The time series of composite vertical wind shear and the composite structure characteristics of TCs during ET are shown in Figs. 4 and 5, respectively. The vertical wind shear was calculated with the method proposed by Palmer and Barnes (2002). It can be found from Fig. 4a and b that the vertical wind shear appears to increase at 24 h before the ET time for both ITC and WTC, suggesting that TCs gradually propagate from the tropical zone to the baroclinic zone. At 12 h before the "ET time", both types of TCs tend to dissipate and their warm cores are not obvious in the low layer. In addition, the ascending motion shifts to the northeast of the TC center (Fig. 5a and d), with the possible reasons as follows: (1). The increasing wind shear caused by the baroclinity in the mid-latitudes can arouse the updraft in the downshear side (northeast side) and the downdraft in the upshear side (southwest side) (Li et al. 2013); (2) The warm front generates on the north of TC and extends eastward under the influence by the encounter of the equatorward cold air from the north of TC with the warm moist airflow poleward on the east of TC. That is, the frontogenesis intends to stimulate the lifting motion.

At Te, as the upper-level trough continues to approach ITC and then they interact with each other, especially when the trough-line extends to the southeast, the u component of wind has somewhat weakened, so the zonal wind shear begins to decrease. However, when the trough is far from the TC and elongates to the southwest, TC will be mainly steered by westerlies in front of trough, inducing the more stable meridional wind shear and the continuously increasing zonal wind shear (Kofron et al. 2010b) (Fig. 4a and d). Simultaneously, the ITC starts to re-intensify with its geopotential height anomaly of −50 gpm, which is 10 gpm lower than that of 12 h before, whereas the WTC weakens with its geopotential height anomaly 10 gpm larger than that of 12 h before. Results also reveal that the negative temperature anomalies of ITC and WTC move eastward and southward, along with the cold air starting to affect TC's outer circulation. Besides, it is worth noting that there are obvious differences of the warm core structures between ITC and WTC. The warm core strengthens at upper and lower levels for the ITC, but almost disappears in the lower layer for the WTC. Compared with the WTC, the temperature in the ITC center is higher than surroundings regardless of the intrusion of cold air. Therefore, the warm core occurs again and the baroclinity somewhat strengthens around the ITC, which is in favor of its reintensification. Thus, the area with large value of vertical wind speed is more close to the center of ITC, but the WTC's vertical motion distribution does not change significantly from the previous 12 h (Fig. 5b and e). At "Te+12", the ITC's total wind shear also tends to decrease, while the WTC is still exposed to the increasing vertical wind shear environment, which is unfavorable for its development (Fig. 4a and b). Kofron et al. (2010b) has pointed out that the reduction of vertical wind shear indicates that the TC and trough are close to each other, while the continuous increase of vertical wind shear implies that the TC remains under the influence of the increasing wind shear associated with the mid-latitude westerlies and never interacts with the upper-level trough. Besides, he fonnd that the maximum intensity of ITC would be achieved after the wind shear decreases based on the composite analysis. At this time, the geopotential height anomaly of the ITC reaches −60 gpm, which is 10 gpm lower than that of 12 h before. Correspondingly, the cold air at the upper level elongates from northwest to southwest of the TC, and intrudes into TC from the southern part at the lower level, but the warm core of the ITC is still kept. To some extent, the "warm seclusion" structure feature is similar to the conceptual model of explosive extratropical cyclone proposed by Shapiro and Keyser (1990). That is, the warm front of cyclone bends back to the rear of the cyclone center, and the warm air near the TC center is encircled by the cold air, which makes the warm core secluded. The ascending motion develops over the ITC center again. The cold air of

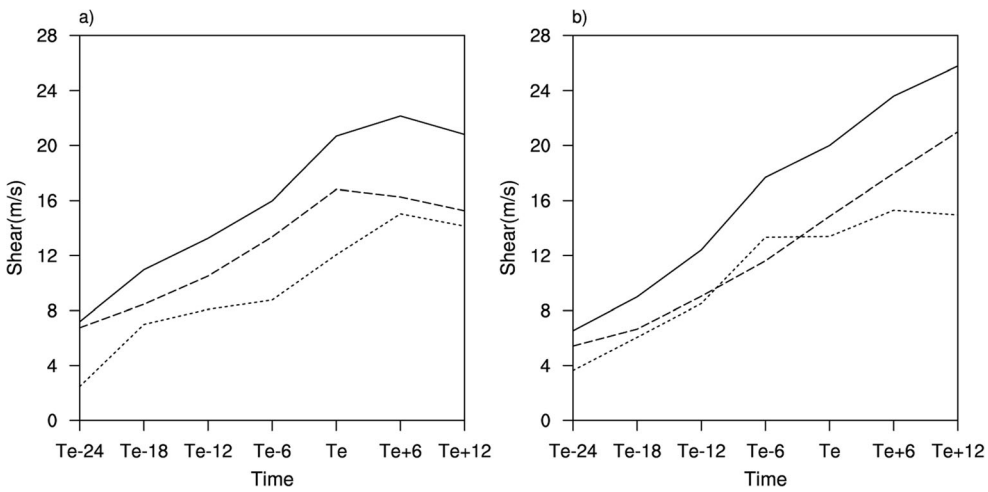

Fig. 4 Time series of composite total vertical wind shear (850–200 hPa, solid line), the u component (long dashed) and the v component (short dashed) of the wind shear for (**a**) ITC and (**b**) WTC

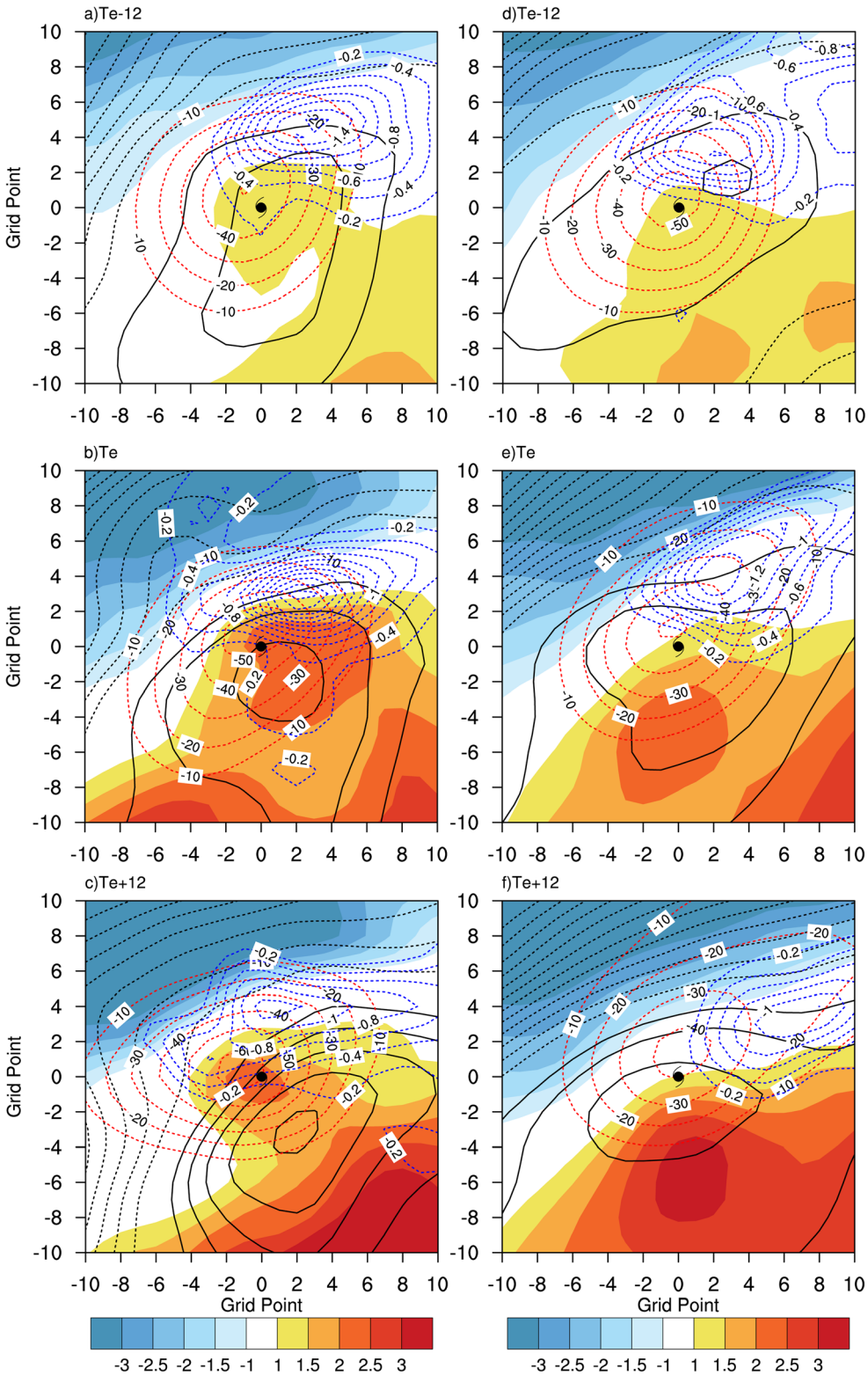

Fig. 5 Composite horizontal distributions of the temperature anomaly (shaded, unit: K) and the vertical wind speed (negative blue dashed contours, interval of 0.2 pa s^{-1}) at 700 hPa, the temperature anomaly at 300 hPa (black solid contours, interval of 0.5 K) and the geopotential height anomaly (red dashed contours, interval of 10 gpm) at 850 hPa for (**a**-**c**) ITC and (**d**-**f**) WTC at the time of (**a**, **d**) Te-12, (**b**, **e**) Te and (**c**, **f**) Te+12

WTC only wanders on the northwest side of TC without further intrusion at both upper and lower levels. Under the influence of increasing vertical wind shear, the updraft of WTC is still limited on the northeast side of TC and gradually moves away from the TC center as the WTC continues to weaken (Fig. 5c and f).

3.3 Mesoscale

In order to present the thermodynamic characteristics of TC inner structure more clearly, the physical fields are investigated at the refined scale of approximately 6° × 6°. Figure 6 shows the

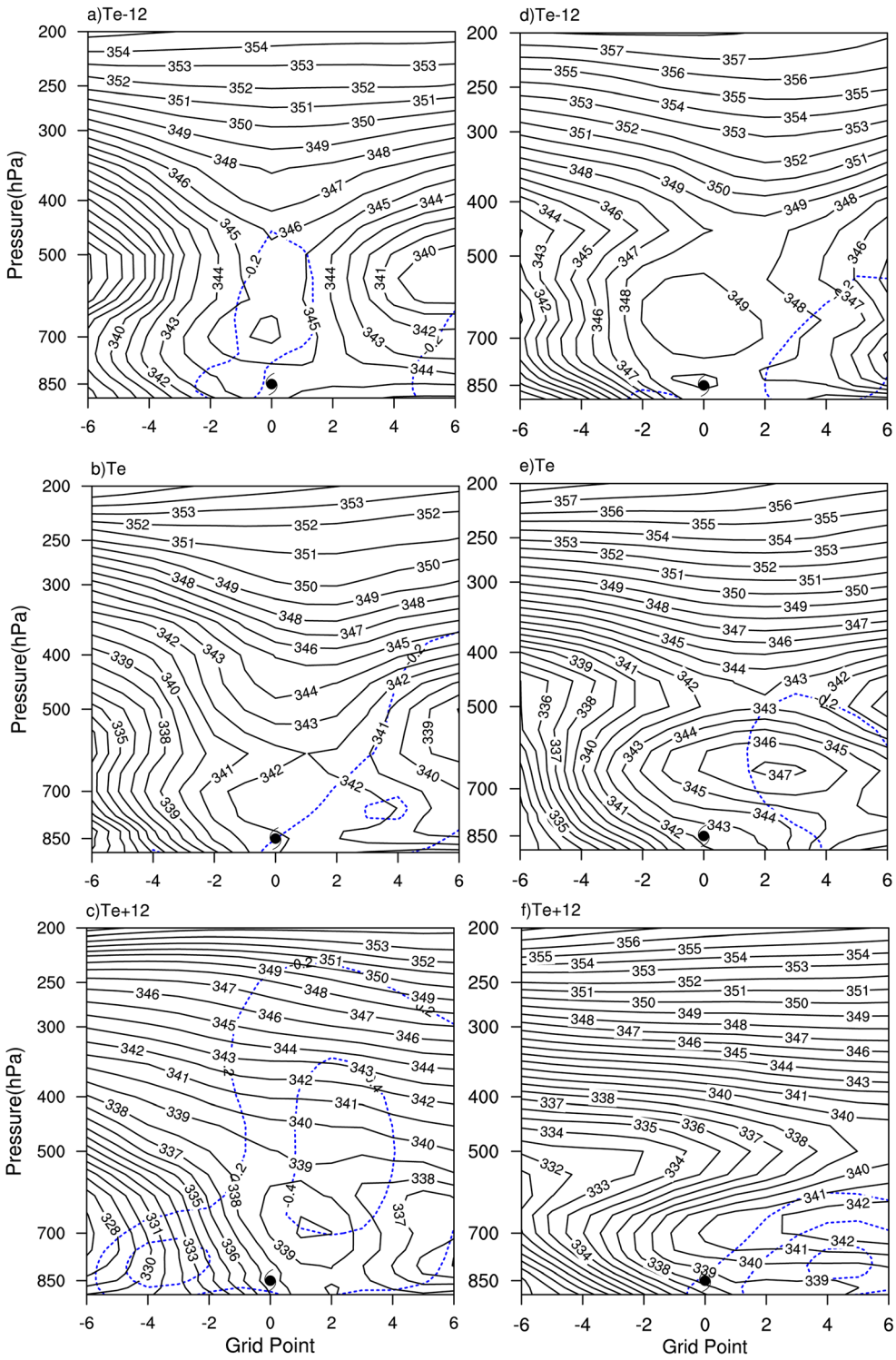

Fig. 6 Composite zonal vertical cross sections of the equivalent potential temperature (black contours, units: K) and the vertical wind speed (negative blue dashed contours, interval of 0.2 pa s^{-1}) of (**a**-**c**) ITC and (**d**-**f**) WTC through the TC center at the time of (a, d) Te-12, (b, e) Te and (c, f) Te+12

zonal vertical section of equivalent potential temperature and the vertical wind speed through the TC center. As depicted in Fig. 6a and d, at "Te-12", there apparently exists a warm core above 700 hPa for the two types of TC, with the more intensified warm core for WTC than ITC. It can be found that the cold air, which is here expressed by lower than 336 K, has not yet intruded into TC for both types of TC, and the strong updraft is located on the northeast (Fig. 5a and d). After 12 h, the warm core of ITC moves downward and the isentropes on the west side of TC become denser at the lower level due to the sharply increasing temperature difference caused by the cold intrusion. Whereas for the WTC case, although there is also cold intrusion marked by <336 K at the lower level, the warm core tends to move eastward. Without the obstacle of the warm core, the middle level of

around 500 hPa is susceptible to the cold intrusion (Fig. 6b and e). At 12 h after the ET time, the' cold air for ITC intrudes further at middle and lower levels and the warm core over the TC center forms again. Therefore, the baroclinity on west of the warm sector strengthens at 500–700 hPa. And the vertical motion near the ITC center develops upward to a higher altitude. Nevertheless, the WTC's warm core continues to move eastward, and thus the cold air further intrudes TC center at the middle level of 500 hPa. Afterwards, the warm core is thoroughly destroyed, and the WTC center seems to be embedded within the equivalent temperature gradient completely. The updraft of WTC inclines to deviate from the TC center and reaches the lower height to some extent (Fig. 6c and f).

4 Dynamic Diagnosis of ITC and WTC

4.1 Moisture Potential Vorticity

The composite horizontal and vertical cross sections of MPV through the TC center are displayed in Figs. 7 and 8. At "Te-12", large MPV values locate over the northwest side of both ITC and WTC at 200 hPa, indicating the upper-level trough over there. At this moment, TC and upper-level trough are independent from each other (Fig. 7a and d). It can be revealed from Fig. 8a and d that the moist isentropes slope downward from the upper-level trough to the TC center, and the MPV to the west side of TC has no obvious downward extension. At

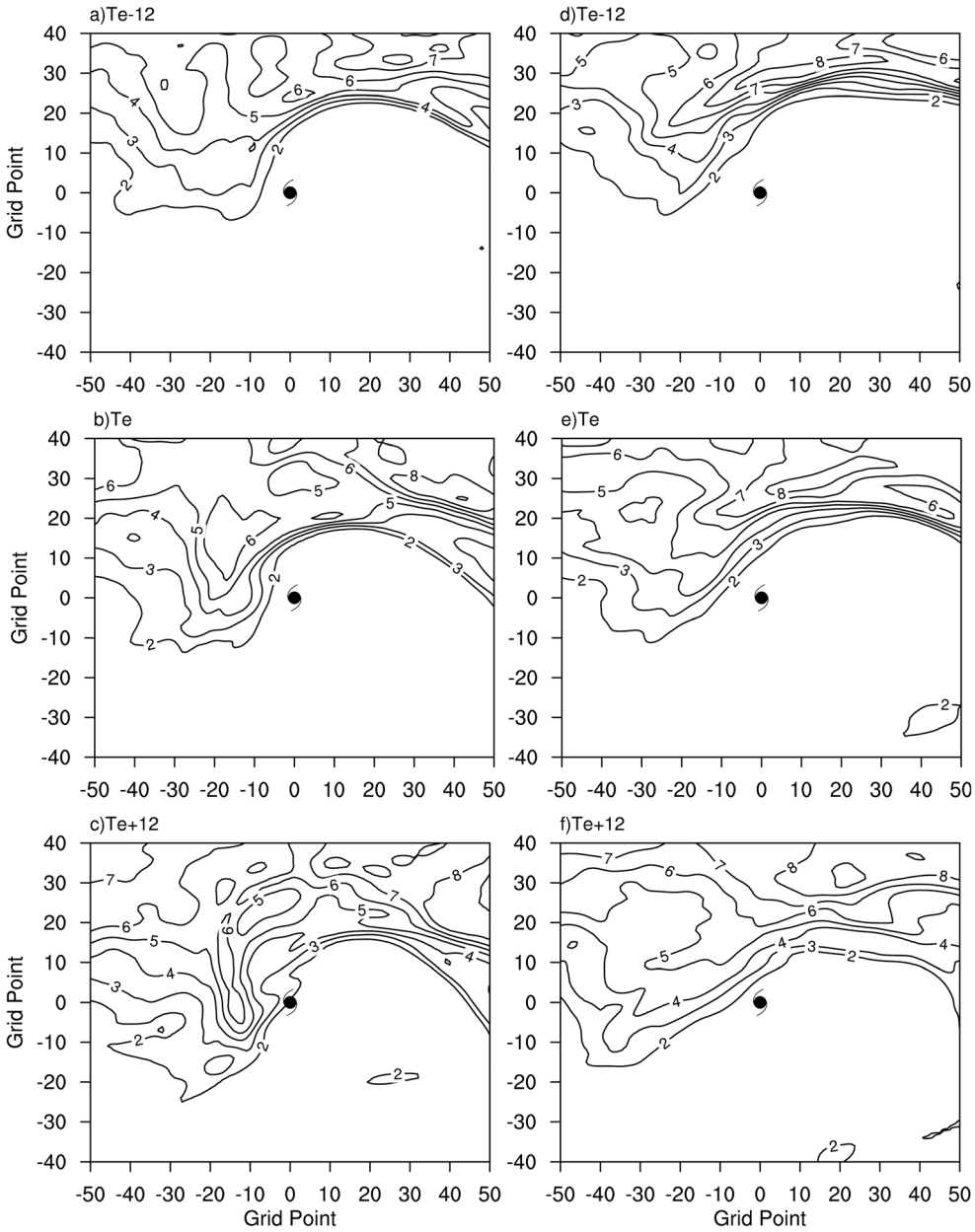

Fig. 7 Same as Fig. 2, but for the MPV at 200 hPa (contours, units: PVU)

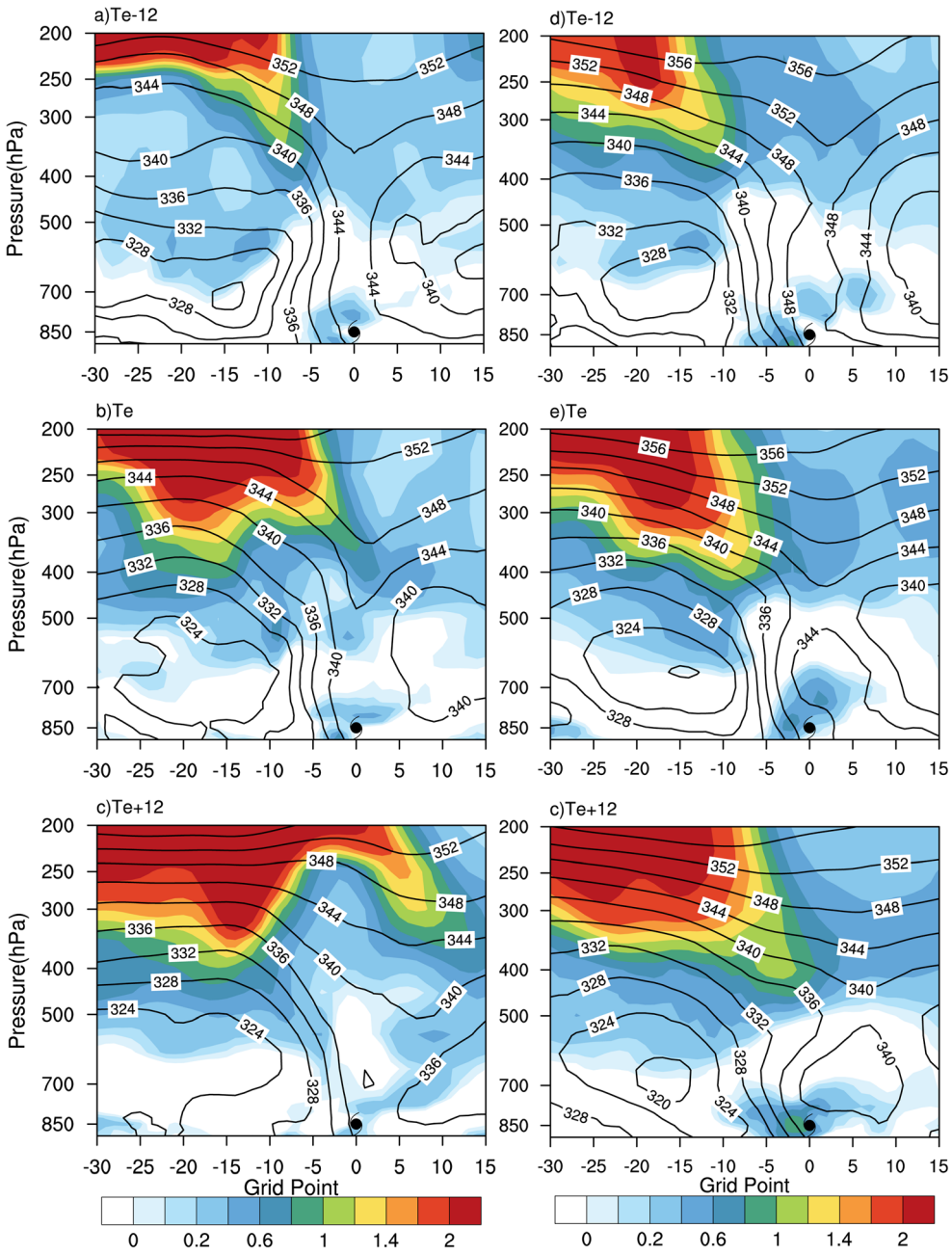

Fig. 8 Composite zonal vertical cross sections of the MPV (shaded, units: PVU) and the equivalent potential temperature (contours, units: K) of (**a**-**c**) ITC and (**d**-**f**) WTC through the TC center at the time of (**a**, **d**) Te-12, (**b**, **e**) Te and (**c**, **f**) Te+12

the ET time, as the trough and TC moving poleward become closer, the maximum center of MPV appears to the northwest of ITC, while the WTC's MPV extends to the southwest and its distribution almost remains the same as the previous 12 h (Fig.7b and 7e). Vertically, the upper-level troughs of both types of TCs deepen, with its MPV greater than 0.4 PVU stretching downward to around 600 hPa where moist isentropes concentrate. The obvious upward bulge of the moist isentropes at 400 hPa on the west side of ITC indicates that the cold air is stacked here, which is not seen in WTC (Fig. 8b and e). After 12 h of ET, with respect to the ITC, the area of large MPV value distributes in the northwest-southeast direction, which is similar to the trough-line at 200 hPa, and extend over the TC center. The WTC's MPV still extends southwestward and has no evident interaction with TC due to the blockage of the South Asia high (Fig. 7c and f). It is also suggested from the vertical cross section that the ITC's MPV transmits downward along the moist isentropes more significantly and is connected with TC, which can transport the MPV to the TC center. The downward transport of cold air with positive MPV leads to the increase of equivalent temperature gradient in their path and the large gradient is closer to the ITC center. However, the standard deviation at the intersection of upper MPV and TC MPV is slightly larger than the average (as shown in Fig. S6 (a) in Online Resource), indicating that the MPV of each sample fluctuates a bit. The reason for it is that 2

of the 5 ITCs have weaker upper-level trough than the other three, resulting in the MPV of the 2 ITCs to fail to transmit downward completely, which implies that the strength of upper-level trough also plays an significant role in TC intensity. For WTC, because of the northeast-southwest trough for WTC, the cold air is advected along the moist isentropes mainly by the westerly around the trough base. As a result, the MPV does not transport downward and the moist isentropes become sparse, indicating the reduced baroclinity (Fig. 8c and f).

To further identify the role of baroclinity in the ET process, the MPV expression is applied in the pressure coordinate (Bosart and Lackmann 1995).

$$MPV = -g(\zeta + f)\frac{\partial \theta_e}{\partial p} + g\left(\frac{\partial v}{\partial p}\frac{\partial \theta_e}{\partial x} - \frac{\partial u}{\partial p}\frac{\partial \theta_e}{\partial y}\right),$$

where g is the gravitation constant, ζ represents the vertical vorticity, the Coriolis parameter f is taken to be constant, θ_e is the equivalent potential temperature, p is the pressure, u and v are the zonal and meridional wind, respectively. The first term on the right side of the equation is the barotropic MPV term (referred as MPV1 hereafter), which is related with inertia stability and convection stability. When MPV1 is greater than 0, it denotes convection stability, otherwise it indicates convection instability. The second term on the right of the equation is the baroclinic MPV term (referred as MPV2 hereafter), which represents the contribution of vertical wind shear and moist baroclinity. MPV2 is usually less than 0 in frontal zone and the greater negative MPV2 value implies the stronger baroclinity. According to the conservation principle of MPV (Wu and Cai 1995), it can has been known that the greater |MPV2| is always accompanied with the greater MPV1. Therefore, the increasing |MPV2| may play a positive role in the variation of vertical vorticity. Figure 9 exhibits time evolution of MPV, MPV2 and vertical vorticity averaged over the 4° × 4° box surrounding the TC center. The ITC's MPV at the upper and lower levels increase obviously after "Te-6", which reflects the influence of the upper-level trough. In view of the distribution of the vertical vorticity and MPV2 for ITC, the moist baroclinity enhances noticeably with time above 400 hPa and below 500 hPa, and the enhancement at lower levels is slightly faster than that at upper levels. Results indicate that the cold air carried by the upper-level trough first intrudes the lower level of ITC along the moist isentropes, leading to the baroclinity increase, then further intrudes the upper level after the trough is closer to the TC. Importantly, the area where the vertical vorticity increases is consistent with that of the moist baroclinity increasing (Fig. 9a). In contrast, no distinct change of MPV is observed at both upper and lower levels for WTC, indicating limited impacts of the upper-level trough on TC. Similarly, the WTC's MPV2 also does not increase obviously with time above 600 hPa. As the WTC weakens continuously, the vertical vorticity above 700 hPa tends to decrease accordingly (Fig. 9b). The comparison on the MPV, MPV2 and vertical vorticity between ITC and WTC shows that the change of baroclinity in TC system caused by upper-level trough will lead to variation of the vertical vorticity to some extent. In order to further study the vertical vorticity variation of ITC and WTC during ET, the complete form of vertical vorticity tendency equation is used to analyze the vorticity budget in the following section.

4.2 Analysis on Complete Form of Vertical Vorticity Budget Equation

Wu (2001) proposed that the traditional vorticity equation deduced from the momentum equation can depict obvious dynamic characteristics. However, real synoptic processes show that severe weather and climate anomalies are usually closely related to atmospheric stability and baroclinity. Therefore, the traditional vorticity equation has limitation for not taking thermal factors into account. Wu and Liu (1999) deduced a complete form of vertical vorticity tendency equation by combining the potential vorticity equation with the vorticity equation. In the condition of no adiabatic and friction, the complete form of vertical vorticity tendency equation taking the TC system as the reference frame under pressure coordinate can be simplified as follows.

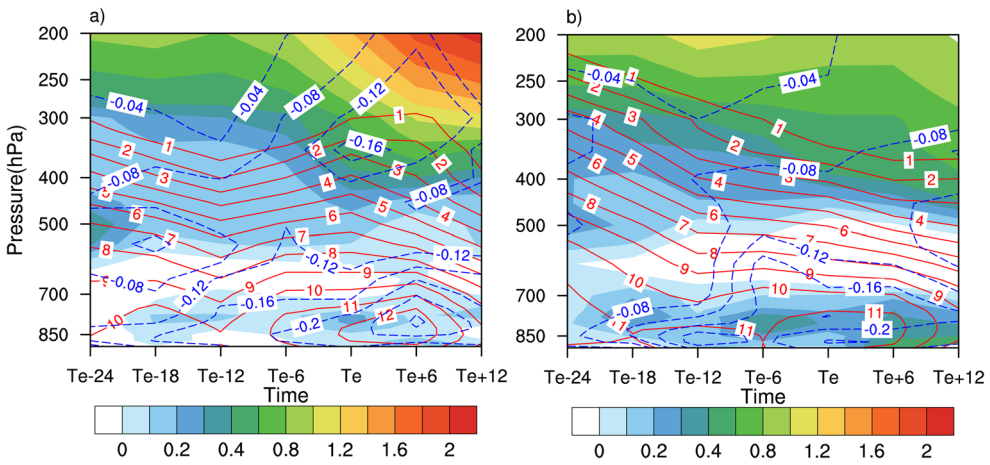

Fig. 9 Composite time-height cross sections of the MPV (shaded, units: PVU), the vertical vorticity (red contours, interval of 1×10^{-5} s^{-1}) and the MPV2 (blue contours, units: PVU) averaged over the 4° × 4° box surrounding the TC center for (**a**) ITC and (b) WTC

$$\frac{\partial \zeta_z}{\partial t} = \left(-\overrightarrow{V_h} + \overrightarrow{C}\right) \cdot \nabla_h \zeta_z - \omega \frac{\partial \zeta_z}{\partial p} - \beta v - \left(\zeta_z + f\right) \nabla \cdot \overrightarrow{V} - \frac{\zeta_z + f}{\theta_{ez}} \frac{d}{dt}(\theta_{ez}) - \frac{\zeta_s}{\theta_{ez}} \frac{d\theta_{es}}{dt} - \frac{\theta_{es}}{\theta_{ez}} \frac{d\zeta_s}{dt},$$

where ζ_z and ζ_s are vertical and horizontal vorticity, respectively, C denotes the moving speed of TC, and f is Coriolis parameter. θ_{ez} and θ_{es} are vertical gradient and horizontal gradient of the equivalent potential temperature, respectively. The first four terms on the right side of the equation are relative vorticity horizontal advection term, vertical advection term, geostrophic vorticity advection term and divergence term, respectively. The last three terms of the equation represent contributions of convective stability variation, baroclinity variation and horizontal vorticity variation associated with vertical wind shear to the vertical vorticity. The geographic vorticity advection and divergence terms are much smaller than the others and the horizontal vorticity variation involves other dynamic processes, and therefore, they are not discussed in this paper. As the moist isentrope lines are nearly perpendicular around TC at the lower level, θ_{ez} is so small that the contributions of stability variation and baroclinity variation to the vorticity vary widely. Therefore, in this paper, we only explored the numerators of these two terms qualitatively, which are the stratification term $-\left(\zeta_z + f\right)\frac{d\theta_{ez}}{dt}$ and the baroclinic term $-\zeta_s \frac{d\theta_{es}}{dt}$.

The horizontal vorticity advection reflects the vorticity redistribution caused by the horizontal wind speed relative to the surface and the movement of TC itself. At "Te-12", the vertical vorticity transport is almost zero for both types of TCs, and there is almost a whole layer of negative horizontal vorticity advection over the WTC center (Fig. 10a and d). As the upper-level trough and TC are close to each other, the upper horizontal vorticity advection to the west side of TC shifts to be positive for both TCs, with the greater intensity and coverage of the positive vorticity advection for the ITC. The strong updraft appears over the ITC center and tends to transport the vorticity from the lower level upward to about 400 hPa, contributing to the increase of vorticity at the middle level. Nevertheless, the vertical vorticity transport is still not evident in the WTC (Fig. 10b and e). At "Te+12", the vertical vorticity transport in the ITC develops more vigorously but it may be effected by an extreme case according to its standard deviation (not shown). The positive horizontal vorticity advection originally located on the west side of ITC moves over the TC center. The upper-level positive vorticity advection can cause the horizontal divergence by the influence of the Coriolis force, which is conductive to the generation of low-level negative pressure anomaly, and simultaneously, it can also contribute to the increase of upper-level vorticity. On the other hand, although there is also positive vorticity advection in the upper level for WTC, their strength and extension are not comparable to those for ITC (Fig. 10c and f).

The contribution of the convective stability variation to the vertical vorticity is reflected in the well-known theory of potential vorticity conservation, namely $q = \frac{\zeta_z + f}{h}$. In the case of stable convection, when the convective stability decreases, the air column thickness increases, inducing the strengthened horizontal convergence and the enhanced vertical vorticity. The significance of the change from moist baroclinity to vertical vorticity is based on the slantwise vorticity development (SVD) theory proposed by Wu and Liu (1999). According to the theory, under the sufficient condition for SVD ($\frac{\zeta_s \theta_{es}}{\theta_{ez}} < 0$), the parcel sliding down along the moist isentropes must be accompanied by $\frac{d\zeta_z}{dt} > 0$. In this paper, we only discuss the variation of θ_e on x-direction due to the analysis of the zonal vertical cross section. As the wind speed increases with height and the equivalent potential temperature on the west side of TC increases along the x-direction, so $\zeta_x \theta_{ex} < 0$ and there is often an area convectively unstable in the lower layer near TC. Therefore, the SVD conditions are met in the middle to upper layers beyond the convectively unstable region. In this paper, we define the baroclinic term as $-\zeta_x \frac{d\theta_{ex}}{dt}$, and $-\zeta_x$ is positive. During the ET process, the stability decreases for both ITC and WTC with the airflows sliding downward along the moist isentropes on the west side, thus contributing to the vertical vorticity. However, the area of large value of stability term is sometimes collocated with the convective instability region or the updraft zone, so it is relatively difficult to clearly explain how the stability term contributes to the intensity change of two types of TCs. At "Te-12", there is distinctly large-value vorticity representing the trough on the west in the upper atmosphere for both ITC and WTC, which is also connected with TC's vorticity. The ITC's own residual vorticity can only reach the level of 400 hPa, while that of WTC can develop up to 200 hPa. At present, there is no distinct change of baroclinity for the two types of TCs (Fig. 11a and d). When the ET just completes, the upper-level vorticity associated with the trough for ITC and WTC increases. The moist isentropes of ITC near the trough have upward bulge, indicating the accumulated cold air over there. As the cold air behind the trough sinks along the moist isentropes, its baroclinity increases, i.e., $\frac{d\theta_{ex}}{dt} > 0$. The increased baroclinity is well collocated with the inclined moist isentropes and corresponds to the increased vorticity between the trough and the ITC. The atmosphere is convectively stable there, thus it is in favor of the development of vertical vorticity. Under the joint effect of the baroclinic term and the vorticity related to the upper-level trough, the ITC's vorticity develops to around 300 hPa. It should be noted that the standard deviation of baroclinity for ITC has the same problem as MPV, that is, the standard

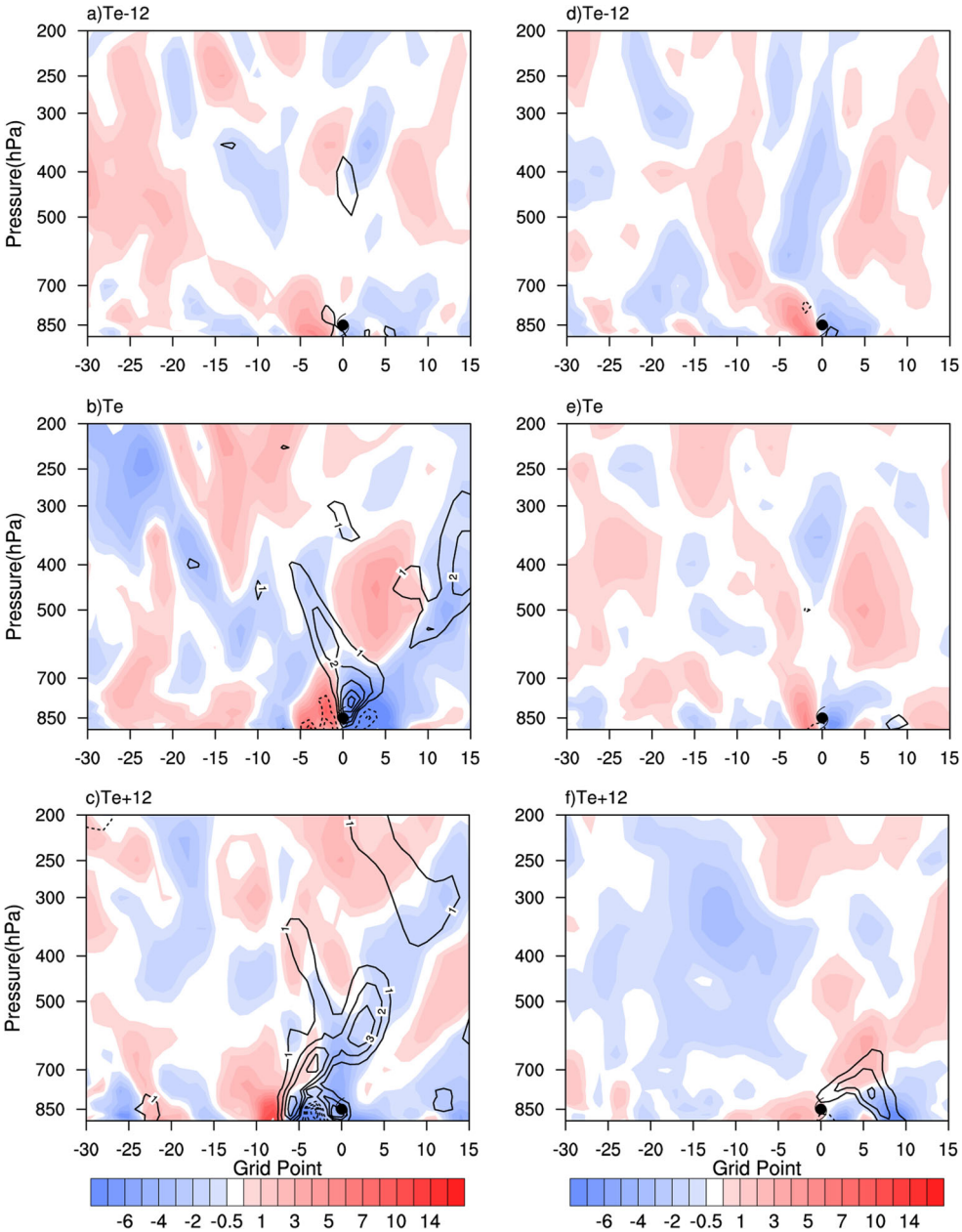

Fig. 10 Same as Fig.8, but for the horizontal vortex advection (shaded, interval of 1×10^{-9} s^{-2}) and the vertical advection (contours, interval of 1×10^{-9} s^{-2})

deviation is slightly larger than the average (as shown in Fig. S8 (a) in Online Resource). After comparing each ITC, we find that the reason for it is the same as MPV: the baroclinity of the two ITCs with weaker troughs hardly contributes to vertical vorticity, which again illustrates the importance of the strength of trough. Although the WTC's vorticity increases at the junction of the upper-level trough and TC, the distance between the trough and TC hardly changes, and the moist isentropes around the trough base in the middle troposphere horizontally distributes with non-significant subsidence of the upper cold air. Therefore, the baroclinic term can be considered with little contribution to the vertical vorticity, reducing the height of WTC's vortex column (Fig. 11b and e). At "Te+12", the ITC's vorticity near the trough is greater than that 12 h ago, and the baroclinic term still contributes to the vertical vorticity. While for the WTC, the vorticity decreases and the baroclinic term has limited contribution to vertical vorticity throughout the ET process, thus the residual vortex column is further destroyed and slopes toward the upper-level trough completely (Fig. 11c and f).

5 Conclusion and Discussion

Two types of TCs with different intensity changes during ET were analyzed by means of composite in the presence of

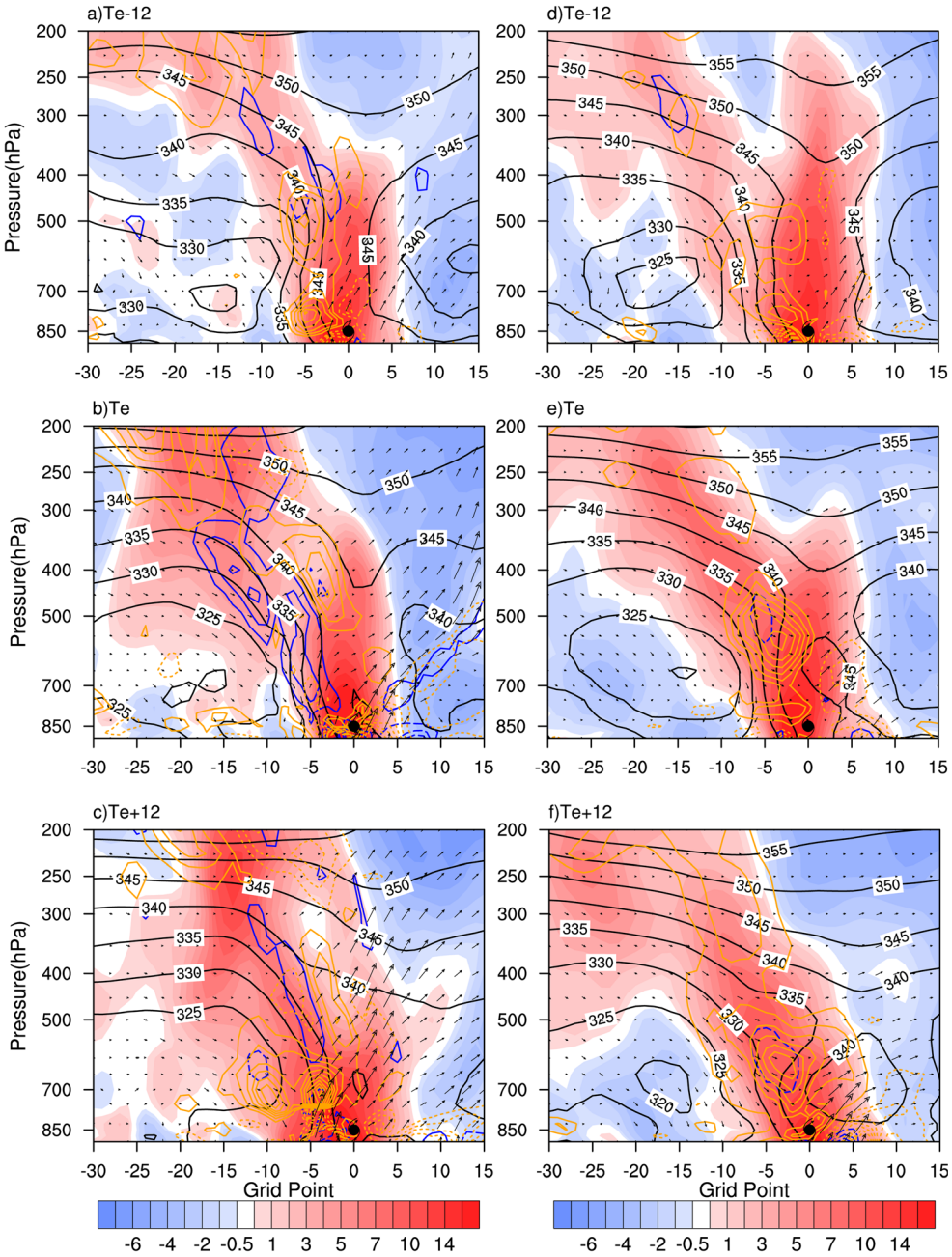

Fig. 11 Same as Fig.8, but for the vertical vorticity (shaded, interval of 1×10^{-5} s^{-1}), the equivalent potential temperature (black contours, units: K), the stratification term (yellow contours, interval of 1×10^{-12} K s^{-2} m^{-1}) and the baroclinic term (blue contours, interval of 1×10^{-12} K s^{-2} m^{-1})

upper-level upstream trough, and the possible mechanisms were discussed by examining large-scale circulation patterns, structure characteristics, MPV and the vertical vorticity budget in this study, which will provide theoretical basis for enhancing the intensity prediction of TCs undergoing ET.

The composite background showed that the South Asia high and subtropical high might have considerable effects on the interaction between the upper-level trough and TC. Due to the blocked South Asia high and subtropical high, the WTC upstream trough was tilted from northeast to southwest. Thus the WTC was mainly steered by westerlies and failed to enter the divergence zone on the right side of the jet entrance. The cold air carried by upper-level trough did not intrude into the TC inner area. On the contrary, the trough for ITC was less affected by the South Asia high or subtropical high and extended toward TC. Therefore, the poleward airflow in front of the trough accelerated the TC to move poleward into the divergence zone.

Before the ET, the warm cores of two types of TCs were destroyed at different levels. In the ET process, as the trough approached, the cold air intruded into ITC, and the cold advection encircled the ITC center in a semi-circular shape, making the warm core occur again. In addition, the decreased wind shear and the enhanced baroclinity also played important roles in ITC's reintensification. While the cold air for WTC only wandered around the northwest side of TC without further

intrusion, its warm core in the lower layer almost disappeared. Affected by the increasing vertical wind shear, the WTC updraft was still confined to the northeast side of TC and gradually moved away from the TC center as the WTC continued to weaken.

MPV distribution at upper level can well reflect the evolution of the trough. The ITC's upper-level MPV gradually extended downward and approached to the TC but it may be closely related to the strength of trough. The downward transport of cold air increased the baroclinity. As a result, the baroclinity of the vortex system at upper and lower levels tended to gradually enhance with time during ET, and then the vertical vorticity increased correspondingly according to the MPV conservation principle. The WTC's MPV elongated toward the southwest alongside the trough-line and did not develop over the TC center or transport downward to the TC vertically. The MPV2 changed slightly with time above 600 hPa, and the vertical vorticity of the whole layer above 700 hPa tended to decrease as a correspondence.

The vorticity budget analysis of ITC and WTC showed that as the upper-level trough and TC were close to each other, the upper-level horizontal vorticity advection to the west side of TC shifted to positive values for both ITC and WTC, and the intensify and coverage of the positive vorticity advection of ITC was greater than that of WTC, leading to the generation of low-level negative pressure anomaly. The contribution of baroclinic term to the growth of vertical vorticity was more significant for the ITC than the WTC but it was also deeply influenced by the strength of upper-level trough.

This paper aims to identify the different effects of the trough on the ITC and the WTC, so the strength of trough is not considered. However, the strength of trough has been proved to have an influence on MPV and baroclinic term associated with TC intensity. Therefore, the strength of trough can be further limited, and this will be studied in the subsequent work. In addition, although the composite analysis is capable of revealing the commonality of TC evolution process, it is unable to connect the dynamic development mechanism with corresponding synoptic processes. Hence, it is necessary to apply the preliminary conclusion obtained from the composite analysis to case analyses to further explore the mechanisms affecting TC intensity variation during the ET process in the future.

Acknowledgments This work was supported by the National Natural Science Foundation of China (Grants 41875070, 41530427 and 41575040) and the Beijige Open Research Fund for Nanjing Joint Center of Atmospheric Research (NJCAR2018MS02) and the Science and Technology Program of Yunnan (2018BC007). The provisions of online data by the China Meteorological Administration (CMA) tropical cyclone database and ECMWF are gratefully acknowledged.

References

Atallah, E.H., Bosart, L.F.: The extratropical transition and precipitation distribution of hurricane Floyd (1999). Mon. Weather Rev. **131**, 1063–1081 (2003)

Baek, E.-H., Lim, G.-H., Kim, J.-H., et al.: Antecedent mid-tropospheric frontogenesis caused by the interaction between a tropical cyclone and midlatitude trough: a case study of typhoon Rusa (2002). Theor Appl Climatol. **118**, 9–24 (2014)

Bosart, L.F., Lackmann, G.M.: Postlandfall tropical cyclone reintensification in a weakly baroclinic environment: a case study of hurricane David (September 1979). Mon. Weather Rev. **123**, 3268–3291 (1995)

Browning, K.A., Thorpe, A.J., Montani, A., et al.: Interactions of tropopause depressions with an extropical cyclone and sensitivity of forecasts to analysis errors. Mon. Weather Rev. **128**, 2734–2755 (2000)

Demirci, O., Tyo, J.S., Ritchie, E.A.: Spatial and spatiotemporal projection pursuit pechniques to predict the extratropical transition of tropical cyclone. IEEE Trans Geosci Remote Sens. **45**, 418–425 (2007)

Evans, J.L., Hart, R.E.: Objective indicators of the life cycle evolution of extratropical transition for Atlantic tropical cyclones. Mon. Weather Rev. **131**, 909–925 (2001)

Harr, P.A., Elsberry, R.L.: Extratropical transition of tropical cyclones over the Western North Pacific. Part I: evolution of structural characteristics during the transition process. Mon. Weather Rev. **128**, 2613–2633 (2000)

Hart, R.E.: A cyclone phase space derived from thermal wind and thermal asymmetry. Mon. Weather Rev. **131**, 585–616 (2003)

Klein, P.M., Harr, P.A., Elsberry, R.L.: Extratropical transition of Western North Pacific tropical cyclones: an overview and conceptual model of the transformation stage. Weather Forecast. **15**, 373–395 (2000)

Kofron, D.E., Ritchie, E.A., Tyo, J.S.: Determination of a consistent time for the extratropical transition of tropical cyclones. Part I: examination of existing methods for finding ``ET time. Mon. Weather Rev. **138**, 4328–4343 (2010a)

Kofron, D.E., Ritchie, E.A., Tyo, J.S.: Determination of a consistent time for the extratropical transition of tropical cyclones. Part II: potential vorticity metrics. Mon. Weather Rev. **138**, 4344–4361 (2010b)

Li Y.: A study on the sustaining mechanism of landfalling tropical cyclones[D]. Ph. D. thesis. Chinese Academy of Meteorological Sciences, Nanjing Institute of Meteorology. (in Chinese) (2004)

Li, K., Xu, H.-M.: The impacts of westerly upper – level trough on the extratropical transition of tropical cyclones landing over China and its possible mechanisms. Chin. J. Atmos. Sci. **36**(3), 607–618 (2012) in Chinese

Li, Y., Chen, L.-S., Lei, X.-T.: Study on rainfall variation associated with typhoon Winnie (9711) during its extratropical transition process. Chin. J. Atmos. Sci. **37**(3), 623–633 (2013) in Chinese

McTaggart-Cowan, R., Gyakum, J.R., Yau, M.K.: Sensitivity testing of extratropical transitions using potential vorticity inversions to modify initial conditions: hurricane earl case study. Mon. Weather Rev. **129**, 1617–1636 (2001)

Niu, B.-S., Ding, Z.-Y., Wang, J.-S.: Development of an explosive cyclone and its relationship with moist potential vorticity. Trans Atmos Sci. **26**(1), 8–16 (2003) in Chinese

Palmer, C. K., and Barnes, G. M., The effects of vertical wind shear as diagnosed by the NCEP/NCAR reanalysis data on northeast pacific hurricane intensity. Preprints, 25th Conf. on Hurricanes and Tropical Meteorology, San Diego, CA, Amer. Meteor. Soc., 122–123 (2002)

Park, D.-S.R., Ho, C.-H., Kim, J.-H., et al.: Highlighting socio-economic damages caused by weakened tropical cyclones in the Republic of Korea. Nat. Hazards. **82**, 1301–1315 (2016)

Ritchie, E.A., Elsberry, R.L.: Simulations of the extratropical transition of tropical cyclones: contributions by the midlatitude upper-level

trough to reintensification. Mon. Weather Rev. **131**, 2112–2128 (2003)

Ritchie, E.A., Elsberry, R.L.: Simulations of the extratropical transition of tropical cyclones: phasing between the upper-level trough and tropical cyclones. Mon.wea.rev. **135**, 862–876 (2007)

Shapiro, M. A., Keyser D.,: Fronts, jet streams and the tropopause. Extratropical Cyclones, the Eric Palmen Memorial Volume, C. W. Newton and E. O. Holopainen, Eds., Amer. Meteor. Soc., 167–191 (1990)

Shou, S.-W.: Theory and application of potential vorticity. Meteor Mon. **36**(3), 9–18 (2010) in Chinese

Shou, S.-W., Li, Y.-H.: Isentropic potential vorticity analysis of the mesoscale cyclone development in a heavy rain process. Acta Meteor Sinica. **59**(5), 560–568 (2001) in Chinese

Thorncroft, C.D., Jones, S.C.: The extratropical transitions of hurricanes Felix and Iris in 1995. Mon. Weather Rev. **128**, 947–972 (2000)

Wu, G.-X.: Comparison between the complete-form vorticity equation and the traditional vorticity equation. Acta Meteor Sinica. **59**(4), 385–392 (2001) in Chinese

Wu, G.-X., Cai, Y.-P.: Moist potential vorticity and slantwise vorticity development. Acta Meteor Sinica. **53**(4), 387–405 (1995) in Chinese

Wu, G.-X., Cai, Y.-P.: Vertical wind shear and down-sliding slantwise vorticity development. Chin. J. Atmos. Sci. **21**(3), 273–282 (1997) in Chinese

Wu, G.-X., Liu, H.-Z.: Complete form of vertical vorticity tendency equation and slantwise vorticity development. Acta Meteor Sinica. **57**(1), 1–15 (1999) in Chinese

Ying, J., Chen, G.-H., Huang, R.-H.: Comparison of intensity changes of western North Pacific tropical cyclones during extratropical transition. Chin. J. Atmos. Sci. **37**(4), 773–785 (2013) in Chinese